Chapter 6

Non linear hyperbolic equation of yolk problem, a practical example

Contents

The chapter provides a numerical closer view to the modeled one dimensional non-linear hyperbolic equation of yolk motion, which is the basis for development of embryo. Amphibian eggs provide several advantageous features as a model system for analyzing the effects of gravity on single cells.

The numerical solution of modeled equation for settling of yolk platelets due to rotation of egg is presented. The wavelet based finite volume approach is utilized with different flux approximations such as Lax–Friedrichs, local Lax–Friedrichs and Roe, to depict the solution with more accuracy. The numerical values are comparable with the solution obtained by the method of characteristics to be an exact one. The study indicates the correspondence between numerical and exact solution and the benefits of combined usage of the numerical approaches to get a better approximation. The L^2 norm and root mean square error for proposed and classical approach is also tabulated for increased grid values to capture the deviations.

The study of yolk platelet motion involves the two-phase flow of yolk and albumin. The article clearly validates the performance of numerical technique in showing the effect of gravitation in the development of embryo. The basic phenomena of the upright phase (first minute), the delay until cortical rotation initiates (up to one hour), and the cortical rotation (30 minutes) are observed in the development process prior to first cell division. The rotation did not significantly affect the temperature distribution of the egg but it was essential for the removal of waste products from near the embryo. The comparison of the solution is made with the solution stated in [10] using method of characteristics and the results depict a better approximation obtained using finite volume method [61] which utilizes the Lax Friedrichs approach and Roe scheme [77] for better accuracy. Graphical comparison is shown for the results.

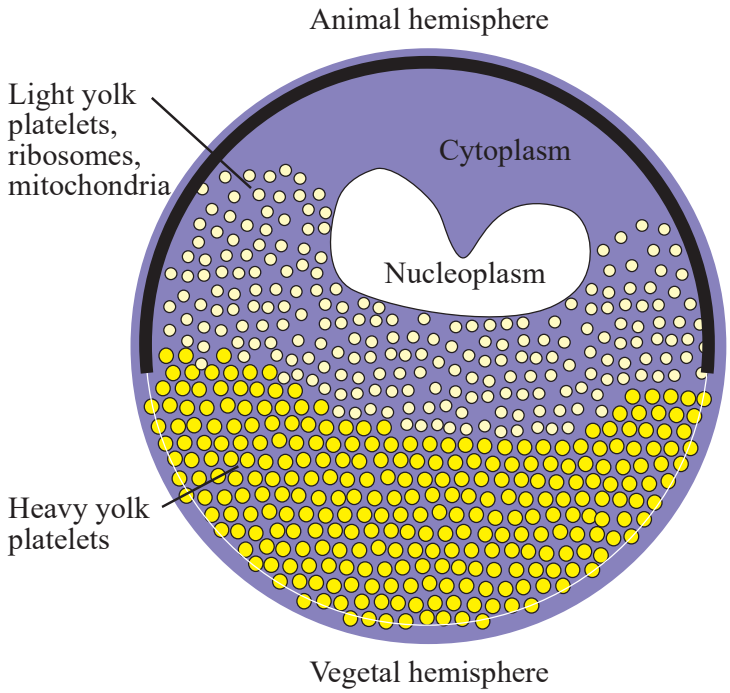

Figure 6.1: Structure of oocyte (from [10])

6.1 Problem background

Bohun [10] has solved the dimensionless simplified mathematical model of two phase flow model for the yolk colloid using method of characteristic. Here a brief discussion is given to further investigate the numerical solution for the same with an improved solution pattern which is validated by the error analysis.

6.1.1 Physical Process

- The periphery is quiet complicated and consist of a series of interconnected layers. Outermost is a layer of follicle cells bounded by follicular epithelium.

- Beneath this is a vitelline envelope and it consist of a network of fibres within

the surface of the plasma membrane with the corticle and pigment granules.

- During the egg fertilization uprighting phase occurs as a result of different yolk densities.

- Asymmetry within egg is introduced by a reorganisation of the cytoplasm at about the halfway point between the moment of fertilization and time of first cell division.

- Gravity plays a role in its development but is paradoxical.

- In the uprighting phase once the egg is fertilized the content of the cortical granules are released into the gap between plasma membrane and vitelline membrane.

- Upon hydration this gap expands to form the perivitelline space, freeing the egg and causing it to rotate.

6.1.2 Governing equations

Mass conservation:

$$\begin{aligned} &\alpha_t + (\alpha u_\alpha)_y = 0, \\ &\beta_t + (\beta u_\beta)_y = 0, \qquad \alpha + \beta = 1. \end{aligned} \tag{6.1.1}$$

Momentum conservation:

$$\underbrace{(-\alpha p_\alpha + \alpha\tau_\alpha)_y}_{\textbf{bulk-average}} + \underbrace{(p_\alpha - \tau_\alpha^{\text{int}})\alpha_y}_{\textbf{surface-average}} - \underbrace{\frac{\mu_\alpha}{a^2}\alpha f(\alpha)(u_\alpha - u_\beta)}_{\textbf{drag of one to another}} + \underbrace{\rho_\alpha g\alpha}_{\textbf{grav.force}} = 0, \quad (6.1.2)$$

$$\overbrace{(-\beta p_\beta + \beta\tau_\beta)_y}^{\textbf{bulk-average}} + \overbrace{(p_\beta - \tau_\beta^{\text{int}})\beta_y}^{\textbf{surface-average}} + \overbrace{\frac{\mu_\alpha}{a^2}\alpha f(\alpha)(u_\alpha - u_\beta)}^{\textbf{drag of one to another}} + \overbrace{\rho_\beta g\beta}^{\textbf{grav.force}} = 0. \quad (6.1.3)$$

where, y is the average inter facial tension; α, β are the volume fraction of yolk and cytoplasm; $u_{\alpha,\beta}$ are speeds of α, β; $p_{\alpha,\beta}$ is averaged isotropic pressure in each phase; g is the acceleration due to gravity; $\tau_{\alpha,\beta}$ are deviatoric stresses constanst; $\tau_{\alpha,\beta}^{\text{int}}$ are the stresses at the interfaces. Also, continuity of stress at the interface between **yolk** and **cytoplasm** is

$$\underbrace{-p_\alpha + \tau_\alpha^{\text{int}}}_{\textbf{yolk}} - \underbrace{(-p_\beta + \tau_\beta^{\text{int}})}_{\textbf{cytoplasm}} = -\gamma\kappa, \quad (6.1.4)$$

here γ is the average interfacial tension; κ is the average interfacial curvature. To close the model four constitutive laws are as follows

$$\tau_{\alpha,\beta} = \mu_{\alpha,\beta}(u_{\alpha,\beta})_y, \ \tau_{\alpha,\beta}^{\text{int}} = -\mu_{\alpha,\beta} f_{1,2}(\alpha,\beta)(u_{\alpha,\beta})_y \quad (6.1.5)$$

where $f_{1,2}$ are functions associated with the geometry of the system and the ease of motion of the liquids.

6.1.3 Dimensionless form

Nondimensionalise the governing equations using the following dimensionless variables (and dropping hats)

$$\begin{aligned} y &= L\hat{y}, \\ u_\alpha &= U\hat{u} = \frac{\rho_\alpha g a^2}{\mu_\alpha}\hat{u}, \\ t &= \frac{L\mu_\alpha}{\rho_\alpha g a^2}\hat{t}, \\ p &= \frac{\mu_\alpha U L}{a^2}\hat{p},\ \varepsilon = \frac{a}{L}. \end{aligned} \tag{6.1.6}$$

A series of algebraic simplifications lead us to

$$\begin{aligned} \alpha_t + (\alpha u)_y &= 0, \\ u &= (1 - p_y)\frac{1-\alpha}{f}, \\ p_y &= \bar{\rho} + (1-\bar{\rho})\alpha \end{aligned} \tag{6.1.7}$$

in otherwords,

$$\alpha_t + \left(\frac{(1-\bar{\rho})\alpha(1-\alpha)^2}{f}\right)_y = 0. \tag{6.1.8}$$

For simplicity $f \equiv 1$, scale $t = \tau/(1-\bar{\rho})$ to remove the explicit dependence on ρ, then yolk problem in dimensionless variables is to solve

$$\alpha_\tau + (\alpha(1-\alpha)^2)_y = 0,\ y \in (0,1),\ \tau > 0,\ \alpha = \alpha(y,\tau) \tag{6.1.9}$$

with initial condition

$$\alpha(y,0) = \alpha_0(y). \tag{6.1.10}$$

The equation is written as,

$$\alpha_\tau + f_1(\alpha)_y = 0, \quad f_1 = \alpha(1-\alpha)^2$$

6.2 Simplified mathematical model

The interior of the egg using a one–dimensional two–phase flow model for the yolk/cytoplasm colloid is shown in figure 6.2. As discussed in [10] the simplified

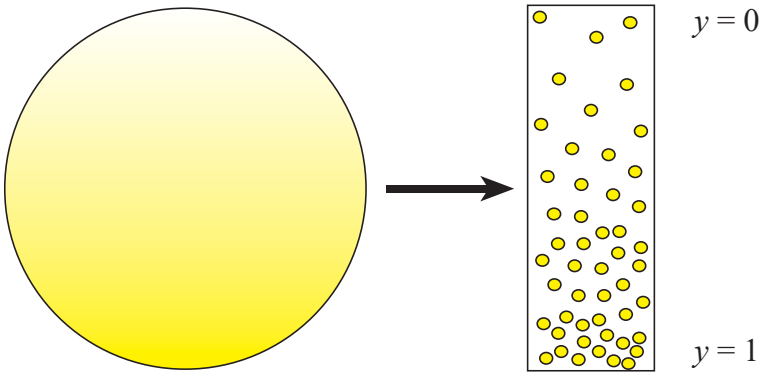

Figure 6.2: One dimensional approximation of interior of the egg from [10]

form of the governing equation which represents α to be the volume fraction of yolk, for average inter facial tension y, with initial condition for settling of yolk from a linear gradient is considered. The equation was given by

$$\alpha_\tau + (\alpha(1-\alpha)^2)_y = 0, \ y \in (0,1), \ \tau > 0, \tag{6.2.1}$$

here $\alpha = \alpha(y, \tau)$. with

$$\alpha(y,0) = y. \tag{6.2.2}$$

and its characteristic solution provided by [10] is of the form,

$$\alpha(y,\tau) = \begin{cases} 0, & 0 \le y < \tau, \\ \frac{1}{6}\left(4 - \frac{1}{\tau} + \sqrt{\left(4 - \frac{1}{\tau}\right)^2 - 12\left(1 - \frac{y}{\tau}\right)}\right), & \tau < y \le 1, \end{cases} \tag{6.2.3}$$

for $\tau < 1/4$. At $\tau = 1/4$ a shock forms and the position of shock was found in [10]. Equation 6.2.1 could be written in a scalar conservation form as,

$$\alpha_\tau + f(\alpha)_y = 0. \tag{6.2.4}$$

with a convex flux function

$$f(\alpha) = \alpha(1-\alpha)^2, \tag{6.2.5}$$

then the choice of numerical scheme must be a conservative one. To satisfy this requirement a finite–volume scheme is a good candidate.

6.3 Finite–volume framework

It is well known [61] that for conservation law equation 6.2.4 with initial condition (IC) equation 6.2.2 a finite–volume framework is as follows:

$$\alpha_\tau = -\frac{1}{h}(\hat{f}_{j+1/2} - \hat{f}_{j-1/2}), \tag{6.3.1}$$

where $\hat{f}_{j\pm1/2}$ is a numerical flux value which one could define in different ways and h is spatial step of discretization. For example [61], the numerical flux in Lax–Friedrichs

(LF) scheme is

$$\hat{f}^{LF}_{j+1/2} = \frac{1}{2}(f(\alpha_j) + f(\alpha_{j+1}) - \sigma(u_{j+1} - u_j)), \quad \sigma = \max_u |f'(u)|,$$

the numerical flux in local Lax–Friedrichs (LLF) scheme is

$$\hat{f}^{LLF}_{j+1/2} = \frac{1}{2}(f(\alpha_j) + f(\alpha_{j+1}) - \sigma_{j+1/2}(u_{j+1} - u_j)), \quad \sigma_{j+1/2} = \max_{(u_j, u_{j+1})} |f'(u)|,$$

and the numerical flux in Roe scheme is

$$\hat{f}^{Roe}_{j+1/2} = \begin{cases} f(u_j), & \sigma_{j+1/2} \geq 0, \\ f(u_{j+1}), & \sigma_{j+1/2} < 0, \end{cases} \quad \sigma_{j+1/2} = \begin{cases} \frac{f(u_{j+1}) - f(u_j)}{u_{j+1} - u_j}, & u_j \neq u_{j+1}, \\ f'(u)|_{u=u_j}, & \text{else.} \end{cases} \tag{6.3.2}$$

Both the Lax schemes are first order scheme, conservative and monotonic were as on the other hand Roe scheme provide more careful solution around discontinuity. At the same time, in recent development of Lax Friedrichs scheme it was noticed that Lax Friedrichs scheme could produce a local oscillations in the numerical solution, as in [27], [66], [38], [3].

6.4 Wavelet and multi resolution revisited

Wavelet is utilized for observing the details, initially the approach of wavelet was widely used in the theory of signal processing and then was extended to the application of differential equations. The phenomena of expressing the function as a linear combination of wavelet bases is utilized to incorporate the properties of multi resolution. The concepts of multi resolution is widely explained in [20], [90]. From [107] the orthogonal projection of a function $f \in L^2[-1, 1]$ onto V_p^n as discussed in

chapter 2 section 2.2 equation 2.2.9 are used.

6.4.1 Algorithm for combined wavelet and finite volume approaches

The algorithm to be as follows:

1. The initial value is projected and decomposed in the wavelet space V_p^n.
2. The finite volume updating is performed to obtain the next time step.
3. The decomposition and reconstruction step is performed with Daubechies wavelet at level of resolution $N = 4$, and then the updating of next time step is performed.
4. Combining the properties of finite volume namely preserving the conservation at each control volume and the multi resolution properties of detailing at each time step helps in improving the accuracy of the proposed algorithm.

6.5 Numerical simulation

The numerical simulation includes the finite–volume approximation of equation 6.2.4 with presence of multi–resolution technique equation 2.2.9. Then initial condition equation 6.2.2 is used in the finite–volume framework equation 6.3.1 with various flux approximations, such as Lax–Friedrichs approach, local Lax–Friedrichs and Roe scheme to depict the function $\alpha(y, \tau)$.

Comparison of exact solution equation 6.2.3 and numerical solution at different

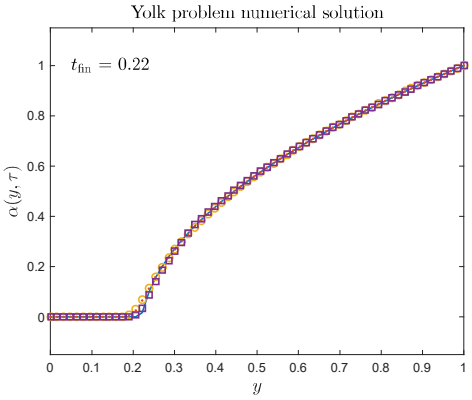

$(a)\tau = 0.22,\ ny = 64$

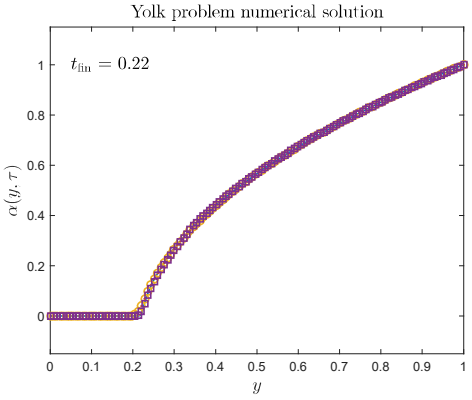

$(b)\tau = 0.22,\ ny = 128$

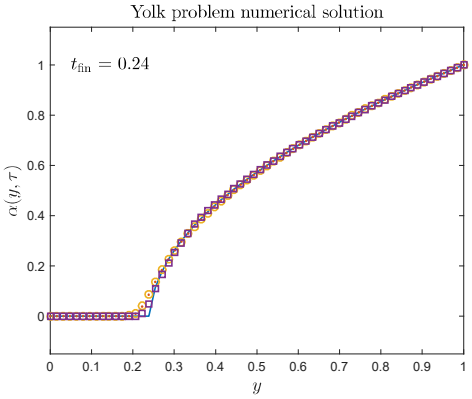

$(c)\tau = 0.24,\ ny = 64$

moments of time t_{fin} with $ny = 64,\ 128$ grid nodes, is obtained. The blue solid is an exact solution, magenta squares is numerical solution by Roe scheme and yellow

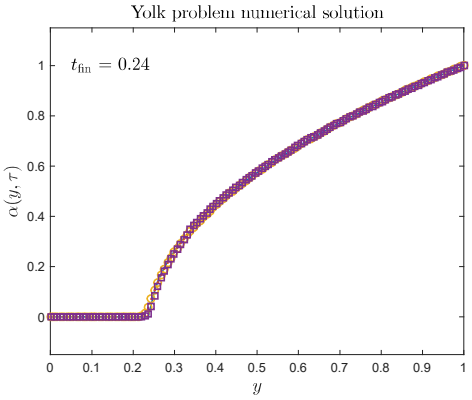

$(d)\tau = 0.24,\ ny = 128$

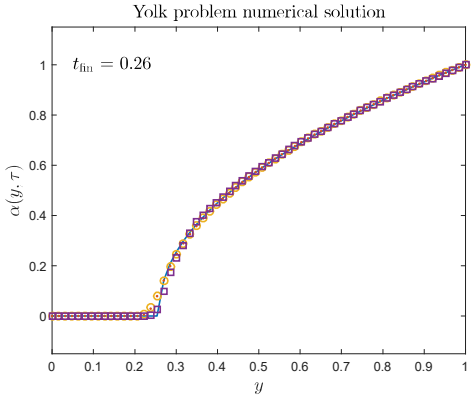

$(e)\tau = 0.26,\ ny = 64$

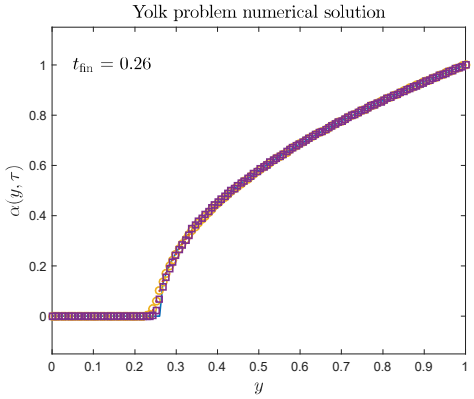

$(f)\tau = 0.26,\ ny = 128$

Figure 6.9: Comparison of solution at different time

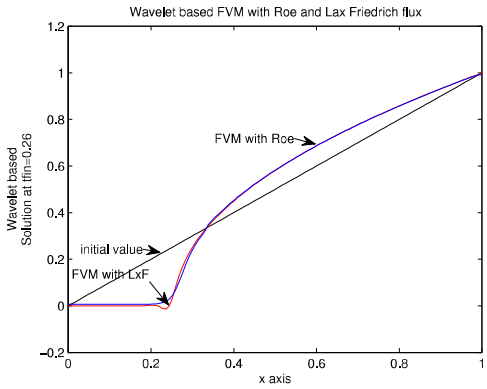

Wavelet based FVM

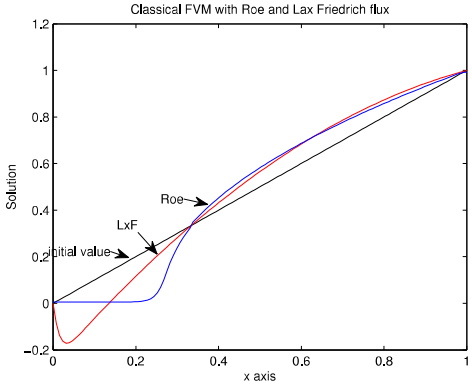

Classical FVM

Figure 6.12: Comparison of wavelet based and classical finite volume

circles is numerical solution by local Lax–Friedrichs scheme in figure 6.9.

The comparison between the classical and proposed wavelet based finite–volume approaches The comparison between the classical and proposed wavelet based finite–volume methods are obtained. The exact, LxF, Roe and initial values of solutions are given in red, blue, green and black respectively in figure 6.12. For computation purpose the computational domain $[a,\, b]$ is normalized as $[0,\, 1]$, ny is the total number of grid points with uniform spatial step length, $h = (b-a)/(ny-1)$ and the Courant–Friedrichs–Lewy number is cfl $= 0.35$, t_{fin} is a final time step.

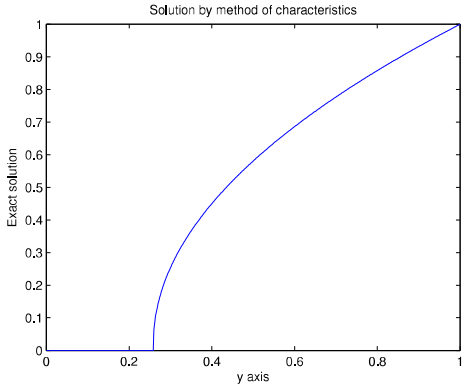

Figure 6.13: Exact solution by method of characteristics

Considering these parameters we obtain all the solution using the three choices of flux function as shown in figure 6.9.

The exact solution equation 6.2.3 is given in figure 6.13 and numerical solution equation 6.2.4, initial condition equation 6.2.2 are shown in figure 6.9 at different moments of time $t_{\text{fin}} = 0.22, 0.24, 0.26$ with $ny = 64$. We considered three values $t_{\text{fin}} = 0.22, 0.24, 0.26$ of time τ around $\tau = 0.25$ in which a shock forms from initial continuous distribution. We would like to notice that in a continuous regime at $t_{\text{fin}} = 0.22$ both three schemes have similar order of L^2 error. Furthermore at $t_{\text{fin}} = 0.24, 0.26$ times, when shock appears and propagates Roe scheme becomes more preferable, because it is more accurate on a shock's front.

Table 6.1: The table gives root mean square error comparison of wavelet based FVM and classical FVM with LxF and Roe performed with exact solution

WFVM	tfin	0.22	0.24	0.26	0.375
wLxF		0.0252	0.0153	0.0022	0.0689
wRoe		0.0244	0.0141	0.0037	0.0689
FVM	tfin	0.22	0.24	0.26	0.375
LxF		0.0654	0.0665	0.0683	0.0884
Roe		0.0244	0.0141	0.0037	0.0689

6.6 Observations

The study justifies that yolk motion is required for the proper development of the embryo and the yolk settling times are consistent with experiments. The upright phase modeled with the simple buoyancy arguments for a low density nucleus trapped inside a viscous cytoplasm and predicts behavior consistent with the observations. The case of linear gradient yolk platelets is solved in a simplest reduced form. The wavelet based finite volume gives a comparable numerical result as per the graph figure 6.9.

In the figure 6.9 the Lax–Friedrichs, local Lax–Friedrichs and Roe approach clearly agrees to the solution. The figure 6.12 gives the comparative plots of wavelet based approach and the classical finite volume approach. The table 6.1 justifies that the proposed approach gives less error as compared to the classical approach which is seen for modified Lax Friedrich in the sense of root mean square error. The values have comparatively less error for both tfin set to values far away from shock as $tfin = 0.375$ and values set to time when the shock is just about to arrive. The modified wavelet based finite volume approach is also tabulated which agrees to the actual value with better accuracy. Although by the table of errors for L^2 we observe that the step size 64 and 128 error remains the same which is an interesting observation. Future research is to still observe the detailed pattern in the phenomenon. The salient feature of finite volume that it needs to evaluate flux for the cell boundaries, combined with the feature of wavelet approximation of detail capturing due to decomposed wavelet approximation of the solution, obtained results are satisfactory.

6.7 Conclusion and Future Scope

The study begins with a proposed unified approach formulation for solving both IVP and BVP using wavelets. A generalization is proposed for random interval with numerical examples. For the approaches Haar wavelet was utilized along with finite difference methodology.

Haar wavelet is used for solving parabolic differential equation where single variable is approximated using wavelet basis. Example solved numerically validates the algorithm implemented. Then to solve elliptic PDE, Haar wavelet is used in two dimension with numerical examples validating the results. Convergence is also observed in root mean square sense for the results obtained.

In the later chapters Godunov finite volume approach is attempted to be combined with wavelet approximation. The wavelet basis like Haar wavelet, Daubechies wavelet and Coiflet wavelets are used with the classical FVM algorithm.

Burger inviscid equation is solved with the proposed approach to study the effect of using combined algorithm. Although the choice of the three wavelet families performed equally well, we could conclude that it is problem specific to choose a wavelet family. Experimental order of accuracy is analysed which uses WFVM and exact solution. It was noted that EOC is improving in WFVM. The benefit of flexibility to analyze the solution due to multiresolution is an added advantage of WFVM.

For viscous Burger equation WFVM is implemented. Numerical examples are solved and compared with already available algorithms in literature. Tabular values are indicated which compares the results for WFVM with algorithms of reproducing kernel function and modified cubic spline method. We could observe that even with courser grid also, satisfactory results were obtained. In another example comparison of WFVM with methods like automatic differentiation and quadratic B-spline method is performed. It was established that even 10 times larger time step gave

desired accuracy which might improve the time complexity of the algorithm. A reconstruction of the function is attempted at a specific resolution. In future alteration of resolution could be attempted.

In the last chapter WFVM is experimented on a yolk model with different flux approximations such as Lax Friedrich, local Lax Friedrich and Roe scheme. We could observe that the solution region which encountered shock could be accurately given using Roe flux approach combined with wavelet approximation. Different final time plots are studied and noted for both WFVM and classical FVM. Lax Friedrich flux approximation clearly depicts improvement due to the combined algorithm in root mean square sense. In future WFVM with varied flux could be attempted with refining of resolution at specific intervals.

The study shows potential areas of application to various partial differential equations involving solutions with shocks.

In future we propose to in corporate refining and thresholding of coefficients of wavelets at the stage of upgradation to the next time step. The study could involve thresholding which could be problem specific . It will lead to fast calculation due to the simplified sparse matrix formulation by neglecting the wavelet coefficients within a specified threshold value fixed by experimental judgement.

In the embryo problem other complex phenomena could be introduced to analyze the solution. A modification of the model could also be experimentally verified using Chebyshev wavelet family.